3868 *Biochemistry* **2010,** *49,* 3868–3878
DOI: 10.1021/bi901458x

BIOCHEMISTRY
including biophysical chemistry & molecular biology
Article

Transition States of Uncatalyzed Hydrolysis and Aminolysis Reactions of a Ribosomal P-Site Substrate Determined by Kinetic Isotope Effects[†]

David A. Hiller, Minghong Zhong,[‡] Vipender Singh, and Scott A. Strobel*

Department of Molecular Biophysics and Biochemistry, Yale University, New Haven, Connecticut 06511
[‡]Current address: AMRI, 26 Corporate Circle, Albany, NY 12203.

Received August 19, 2009; Revised Manuscript Received March 30, 2010

ABSTRACT: The ester bond of peptidyl-tRNA undergoes nucleophilic attack in solution and when catalyzed by the ribosome. To characterize the uncatalyzed hydrolysis reaction, a model of peptide release, the transition state structure for hydrolysis of a peptidyl-tRNA mimic was determined. Kinetic isotope effects were measured at several atoms that potentially undergo a change in bonding in the transition state. Large kinetic isotope effects of carbonyl ^{18}O and α-deuterium substitutions on uncatalyzed hydrolysis indicate the transition state is nearly tetrahedral. Kinetic isotope effects were also measured for aminolysis by hydroxylamine to study a reaction similar to the formation of a peptide bond. In contrast to hydrolysis, the large leaving group ^{18}O isotope effect indicates the C−O3′ bond has undergone significant scission in the transition state. The smaller carbonyl ^{18}O and α-deuterium effects are consistent with a later transition state. The assay developed here can also be used to measure isotope effects for the ribosome-catalyzed reactions. These uncatalyzed reactions serve as a basis for determining what aspects of the transition states are stabilized by the ribosome to achieve a rate enhancement.

The ribosome catalyzes two chemical reactions during protein synthesis. During initiation and elongation, peptide bonds are formed by the nucleophilic attack of an aminoacyl-tRNA in the A-site on peptidyl-tRNA in the P-site. During termination, water acts as the nucleophile, resulting in the release of the peptide chain from tRNA. The ribosome must be capable of selectively switching between these two catalytic activities, since hydrolysis during elongation would produce truncated proteins, and peptide bond formation in place of termination would result in read-through of stop codons.

In the past decade, a wealth of structural information has been obtained to complement the biochemical study of catalysis by the ribosome. Structures of the 50S ribosome demonstrated that the active site for peptide bond formation is composed entirely of RNA (*1*, *2*). Of the functional groups present in the active site, two have been identified as being important for catalysis of peptide bond formation: the 2′-hydroxyl of A2451 in 50S RNA contributes ~10-fold (*3*), and the 2′-hydroxyl of the terminal adenosine of peptidyl-tRNA, which is adjacent to the leaving group, contributes at least 10^6-fold (*4*). Brönsted (*5*) and kinetic isotope effect studies (*6*) indicate that the nucleophilic nitrogen is neutral in the transition state despite at least partial peptide bond formation. More recently, structures of 70S ribosomes bound to either release factor 1 (*7*) or release factor 2 (*8*, *9*) have shown the location of the conserved GGQ motif in the active site for peptide release. Mutational studies showed that both glycines are essential, while the side chain of glutamine is only moderately important (*10*−*13*).

In both peptide bond formation and hydrolysis, the electrophile is a peptidyl-tRNA bound in the P-site of the ribosome. The growing peptide chain is linked to tRNA as a carboxylic acid ester through the 3′-hydroxyl of the terminal adenosine. The reactivity of similar carboxylic acid derivatives has been studied extensively. Isotope effects (*14*) and pH dependence studies (*15*) have been used to probe proton transfer. Structure−reactivity and linear free energy relationships such as Brönsted studies have also been performed (*16*−*18*). Oxygen exchange experiments using isotopic labels have been invaluable in establishing the existence of a tetrahedral intermediate and identifying the rate-limiting step (*19*).

Detailed knowledge of uncatalyzed reactions serves as a basis for understanding enzymatic catalysis. The structure of the transition state is particularly informative, since enzymes increase the reaction rate by lowering the energy of this state. Because transition states cannot be viewed directly, measuring kinetic isotope effects is a valuable strategy for determining transition state structures (*20*, *21*). The rate of a chemical reaction may change upon substitution of an atom at the reaction center with a heavier isotope. This effect is dependent on the change in bonding to that atom from the ground state to the transition state. Therefore, given a ground state structure and kinetic isotope effects for several substitutions, the structure of the transition state can be determined.

We have previously reported the synthesis of a set of molecules needed for kinetic isotope effect analysis of the reactions of a ribosomal P-site substrate (*22*, *23*). In this study, we have determined the transition states for the uncatalyzed hydrolysis and aminolysis of this substrate. These structures indicate possible roles for the ribosome in catalyzing the two reactions of protein synthesis.

[†]This research was supported by National Institutes of Health (NIH) Grant GM54839 (to S.A.S.), NIH Postdoctoral Fellowship GM079980 (to D.A.H.), and a Brown-Coxe fellowship (to V.S.).

*To whom correspondence should be addressed. Telephone: (203) 432-9772. Fax: (203) 432-5767. E-mail: scott.strobel@yale.edu.

 Published on Web 04/01/2010 © 2010 American Chemical Society

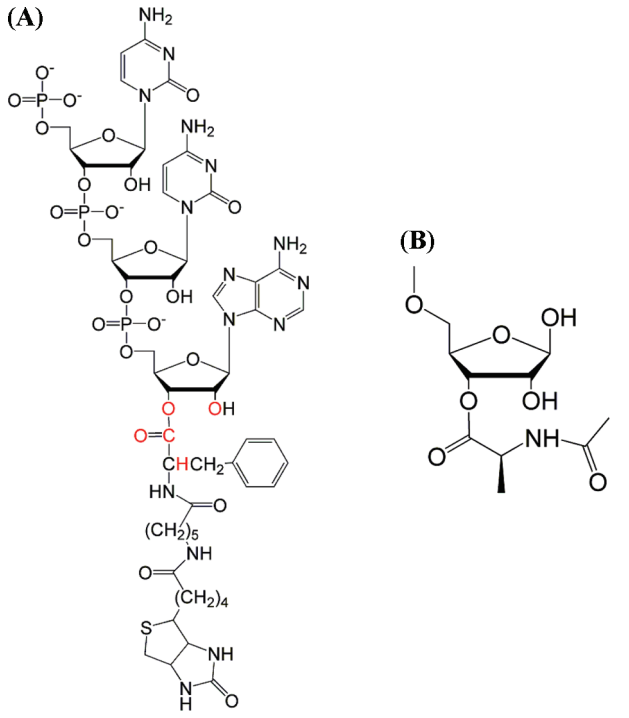

FIGURE 1: (A) Structure of the ribosomal P-site substrate CCApcb with 5′-phosphate (either ^{32}P or ^{33}P). Positions of the individual isotopic substitutions are colored red. (B) Simplified model used for calculating isotope effects.

EXPERIMENTAL PROCEDURES

Reactant Preparation. Reactants differing only by single isotopic substitutions at the reaction center were prepared for isotope effect studies (Figure 1). The P-site mimic cytidylyl-(3′5′)-cytidylyl-(3′5′)-3′(2′)-*O*-{*N*-[6-D-(+)-biotinoylaminohexanoyl]-L-phenylalanyl}adenosine (CCApcb)[1] was synthesized as described previously (*22*, *23*) and stored at −80 °C until it was used. It was resuspended in 50 mM TEAA (pH 6.5) and purified from hydrolyzed material (CCA) by HPLC on a C-18 column using a gradient from 0 to 40% acetonitrile. The HPLC peak was lyophilized, resuspended in 2 mM MES (pH 5.5), and 5′-end labeled with either [γ-^{32}P]- or [γ-^{33}P]ATP by polynucleotide kinase. Labeling reactions were conducted for 5 min at room temperature and pH 6.5 to reduce the level of hydrolysis. Labeled CCApcb was purified on a pH 6.0 denaturing 15% polyacrylamide gel, and gel slices were eluted into 2 mM MES (pH 5.5). [^{32}P]- and [^{33}P]CCApcb were mixed at an approximately 1:4 ratio and purified on a pH 6.0 nondenaturing 12% polyacrylamide gel. Gel slices were again cut out and eluted into 2 mM MES (pH 5.5). Purified mixes were used as soon as possible to minimize hydrolysis in the starting material.

The isotopic enrichment of each sample was determined by high-resolution Fourier transform ion cyclotron resonance mass spectrometry. The molecule was resuspended in a 1:1 water/acetonitrile mixture and analyzed in negative ion mode. The average value of peaks corresponding to both the −1 and −2 charge states was used. Each molecule was ≥95% isotopically pure except for the carbonyl ^{18}O substitution, which was 74% enriched.

[1]Abbreviations: CCApcb, cytidylyl-(3′5′)-cytidylyl-(3′5′)-3′(2′)-*O*-{*N*-[6-D-(+)-biotinoylaminohexanoyl]-L-phenylalanyl}adenosine; KIE, kinetic isotope effect; EIE, equilibrium isotope effect; FLB, formamide loading buffer.

The equilibrium ratio of 2′- to 3′-linked ester was determined by ^{1}H NMR. CCApcb was suspended in 5 mM Tris (pH 8.5), lyophilized, and resuspended in 99.990% D_2O at approximately 500 mM. A one-dimensional spectrum was collected immediately. The sample was then allowed to hydrolyze over several days, and another spectrum was collected to assist in peak identification. Two peaks in the adenosine H1′ region were present in the unhydrolyzed but not the hydrolyzed sample. On the basis of previous studies and the chemical shift rule, the downfield peak was assigned to the 2′-linked isomer (*24*−*26*) and the ratio of the two peaks was used to determine the isomeric ratio.

Identity of the Nucleophile in the Hydroxylamine Reaction. The reaction of CCApcb with hydroxylamine was observed by ^{13}C NMR. CCApcb labeled at the carbonyl carbon was suspended in 10% D_2O to a concentration of approximately 2 mM. Hydroxylamine was diluted to a 5 M stock solution and brought to pH 8.5 with HCl. Hydroxylamine was added to a final concentration of 250 mM, and the reaction was quenched with 5% formic acid after approximately 1 min. Alternatively, 500 mM hydroxylamine or 50 mM HEPES (pH 8.5) was added, and these reactions were quenched with 5% formic acid after 1 day. The ^{13}C spectrum of each sample as well as starting material (again with 5% formic acid) was collected for 12 h.

Samples of CCApcb before and after reaction with hydroxylamine were subjected to a ferric chloride test for hydroxamic acid. To approximately 2 mM CCApcb was added 1/10 volume of either 5 M hydroxylamine (pH 8.5) or water. HCl and $FeCl_3$ were added to each sample to final concentrations of 100 mM and 0.05%, respectively, and the absorbance spectra were recorded with a NanoDrop 2000c spectrophotometer.

Hydrolysis Isotope Effect Reactions. Reactions were started via addition of $^{1}/_{10}$ volume of 10× ribosome reaction buffer [final concentrations of 25 mM HEPES, 10 mM MES, 10 mM MOPS, 200 mM NH_4Cl, and 7 mM $MgCl_2$ (pH 8.5)] at 25 °C. Most of the reaction was quenched at approximately 20% reacted (approximately 2 h) via addition of 3 volumes of low-pH formamide loading buffer (FLB) and freezing at −20 °C. The remainder was allowed to react for at least 36 h to reach completion. Both time points were run on a pH 6.0 denaturing 15% polyacrylamide gel to separate substrate from product.

Substrate and product bands were visualized using a Storm 840 PhosphorImager with a two-ply sheet of duck tape between the gel and screen to block ^{33}P emission. The fraction of ^{32}P-labeled substrate reacted could then be determined. The ratio of ^{32}P to ^{33}P was determined by scintillation counting. Each product band was excised from the gel and eluted into 1 mL of water overnight. This water was then added to 13 mL of Optima Gold scintillation fluid and counted for 30 min along with ^{32}P and ^{33}P standards.

Aminolysis Isotope Effect Reactions. Reactions with hydroxylamine were conducted as described for the hydrolysis reaction with the following exceptions. Reactions were initiated via addition of $^{1}/_{10}$ volume of 5 M hydroxylamine (pH 8.5). Time points were quenched after approximately 5 min via addition of 2.5 volumes of FLB and immediately loaded onto a prerunning gel. The remainder of the reaction was allowed to proceed for 1−2 h.

Data Analysis. Counts per minute were divided into two channels, 0−400 and 400−2000 keV. Approximately 70% of the ^{32}P standard was detected in the high-energy channel, and more than 99% of the ^{33}P sample was detected in the low-energy

channel. The ratio of ^{32}P to ^{33}P in each sample could be determined using eq 1:

$$\frac{^{33}P}{^{32}P} = \frac{A - Br}{B(1+r)} \quad (1)$$

where A is the number of counts per minute in the low-energy channel, B is the number of counts per minute in the high-energy channel, and r is the fraction of total emission of a ^{32}P standard detected in the low-energy channel. The observed isotope effect was then determined from the ratio in the midpoint and end point samples and the fraction reacted using eq 2:

$$\mathrm{KIE} = \frac{\log(1-f)}{\log\left(1 - \frac{fR_p}{R_0}\right)} \quad (2)$$

where f is the fraction reacted, R_p is the isotope ratio in the product at that fraction reacted, and R_0 is the isotope ratio in the product at the reaction end point. For high-fraction reacted samples (>50%), the isotope effect was also determined from substrate and end point samples using eq 3:

$$\mathrm{KIE} = \frac{\log(1-f)}{\log\left[\frac{(1-f)R_s}{R_0}\right]} \quad (3)$$

where R_s is the isotope ratio in the remaining substrate at f fraction reacted and R_0 is the same as described above. This value was corrected for incomplete isotopic incorporation as determined by mass spectrometry with eq 4:

$$\mathrm{KIE}_{\mathrm{corrected}} = 1 + \frac{\mathrm{KIE}_{\mathrm{observed}} - 1}{1 - \mathrm{KIE}_{\mathrm{observed}}(1-e)} \quad (4)$$

where e is the isotopic enrichment of the heavy sample. This equation assumes a negligible amount of heavy isotope in the light sample (*27*).

Since kinetic isotope effects are ratios of rates, the geometric mean and standard deviation are the correct statistics for describing the data. However, the arithmetic and geometric means and standard errors were equivalent for these sets of data, and for the sake of clarity, the arithmetic versions are presented. The means and standard errors were similar whether each measurement was treated as independent or whether multiple trials with the same reactant mix at the same time were averaged and treated as a single measurement. The total number of trials is listed with each value.

Hydrolysis Kinetics. The rate effect of the 2′-deoxyadenosine substitution in CCApcb was determined in side-by-side reactions. Reactions were started via addition of $^1/_{10}$ volume of 10× ribosome reaction buffer. The reaction was quenched via addition of 4 volumes of FLB.

The overall solvent isotope effect was determined via replacement of H_2O in the reaction mixture with D_2O. Since the radiolabeled CCApcb and 10× reaction buffer were kept in H_2O, the reaction mixture contained 85% D_2O.

In all cases, plots of fraction reacted versus time fit to a single exponential (eq 5):

$$f = (f_\infty - f_0)(1 - e^{-k_{obs}t}) + f_0 \quad (5)$$

where f is the fraction reacted at time t, f_∞ is the fraction reacted extrapolated to infinite time, f_0 is the fraction reacted at time zero, and k_{obs} is the observed rate of hydrolysis. For the 2′-deoxy reactant, less than 20% reacted within approximately 3 days. Therefore, the fraction reacted at infinite time was fixed to the same value as for the ribose reactant.

Computation of Transition States. Transition state structures for the hydrolysis and aminolysis reactions that reproduced the experimental KIEs were determined in vacuo using hybrid density functional methods implemented in Gaussian03 (*28*) using the model tetrahydro-4,5-dihydroxy-2-(methoxymethyl)-furan-3-yl 2-acetamidopropanoate. Structures of the transition states were optimized and the frequencies computed on the optimized structures using the three-parameter Becke (B3) exchange functional, the LYP correlation functional, and the standard 6-31G(d,p) basis set. The 5′-methoxy group and the reaction center were constrained during the optimization, and many of these constraints were modified to match the experimental KIEs.

Kinetic and equilibrium isotope effects (KIEs and EIEs, respectively) were calculated from the computed frequencies using ISOEFF 98 (*29*). KIEs and EIEs were calculated at 298 K, and the frequencies were scaled using a factor of 0.964, corresponding to the B3LYP/6-31G(d,p) basis set. All vibrational modes were used to calculate isotope effects. We generated geometric and electrostatic models by iteratively optimizing the transition states by modifying the applied constraints until the computed isotope effects closely match the experimental KIEs. Isoeff98 uses an imaginary frequency of 50i cm^{-1} as a cutoff for calculating KIEs versus EIEs. KIEs were calculated when the magnitude of the imaginary frequency which contained some contribution from the reaction coordinate was greater than 50i cm^{-1}, indicating partial bond orders. Conversely, when significant or full bond orders were observed at the transition state, either a small (imaginary frequency of < 50i cm^{-1}) or no imaginary frequency was observed corresponding to the reaction coordinate. In this case, the transition state was treated as an intermediate and equilibrium isotope effects were calculated. Experimental KIEs predicted full bond orders for the hydrolysis reaction with the transition state resembling the tetrahedral intermediate. The hydrolysis reaction was therefore modeled as an intermediate, and EIEs were matched to the experimental KIEs. The aminolysis reaction had experimental KIEs that suggested partial bond orders; therefore, it was modeled as a transition state, and KIEs were calculated. The final model that is consistent with the experimental KIEs had multiple imaginary frequencies. All frequencies were used for calculating KIEs.

The natural bond orbital (NBO) calculations were performed on optimized structures by including the pop = nbo keyword in the route section of input files. The molecular electrostatic potential (MEP) surfaces were calculated by the CUBE subprogram of Gaussian03. The formatted checkpoint files used in the CUBE subprogram were generated by constrained geometry optimization at the B3LYP level of theory with the 6-31G** basis set. MEP surfaces of the substrate and the transition states were visualized using Molekel4.0 at a density of 0.008 electron/a_0^3.

RESULTS

Measurement of Isotope Effects by the Remote Label Method. Kinetic isotope effects can be used to determine the structure of the transition state of a chemical reaction (reviewed in refs *20* and *21*). To conduct these studies, reactants must be prepared that differ only in the isotope at a particular position of

interest. The rate effect for a single isotopic substitution is related to the change in bond order of that atom between the ground state and the transition state. If several substitutions are made individually, the change in bond order of each atom can be determined and a complete map of the transition state can be constructed. A synthetic strategy amenable to isotopic substitution was developed for a compound that mimics the peptidyl-tRNA that is bound to the ribosome during protein synthesis (*22*, *23*). To improve our understanding of its reactivity to nucleophilic attack, kinetic isotope effects were determined for the uncatalyzed hydrolysis and hydroxylaminolysis of this substrate. These reactions mimic peptide release and peptide elongation reactions catalyzed by the ribosome, respectively.

Because heavy atom kinetic isotope effects are generally very small (usually a few percent or less), it was impractical to determine them by independently measuring the reaction rates of the substituted and unsubstituted compounds. Instead, a competitive reaction was employed, in which the two compounds were mixed and the isotope effect was determined by the relative enrichment of one compound in either the substrate or product. The compound with the faster-reacting isotope was enriched in the product and depleted in the substrate, and the opposite was true for the slower-reacting isotope.

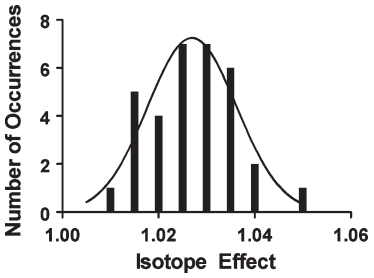

FIGURE 2: Histogram of ^{13}C kinetic isotope effects on aminolysis. The data set fits to either a log-normal (shown) or normal distribution.

Since the two compounds were present in the same reaction mixture, a remote radiolabel was used to differentiate them. The substituted and unsubstituted molecules were labeled at the 5′-end with a phosphate containing either ^{32}P or ^{33}P. Since the emission energies of the two radiolabels differ by approximately 7-fold, they can be distinguished by scintillation counting. An added benefit of this strategy was the flexibility of labeling either compound with either radioisotope. Therefore, the isotope effect was measured by pairing the light isotope with ^{32}P and the heavy isotope with ^{33}P, and again by pairing the heavy isotope with ^{32}P and the light isotope with ^{33}P. This radiolabel pair was previously used to determine a kinetic isotope effect on a 4-thiouridine synthase ribozyme (*30*). The ease of labeling with polynucleotide kinase and the availability of two radioisomers of phosphorus make this radiolabel pair particularly useful for the determination of kinetic isotope effects for enzymes with oligonucleotide substrates.

To evaluate the precision and reproducibility of the assay, we determined the primary isotope effect (^{13}C substitution at the carbonyl carbon) 33 times for the aminolysis reaction. A histogram of the data is consistent with a log-normal distribution as expected for repeated measurements of ratios (Figure 2). Furthermore, repeated trials on different days gave the same effect within error. Measurements at different fractions reacted, as well as using either substrate or product to determine the isotope effect, all gave the same effect. Finally, the isotope effects due to the purification and counting procedure or for the remote label were also within the error of the experiment.

Reaction Pathway of Hydrolysis of CCApcb. A simple mechanism for hydrolysis involving only the formation and breakdown of a tetrahedral intermediate was used as a framework for interpreting isotope effects (Figure 3). The observed isotope effect is dependent on the individual effects on k_1, k_{-1},

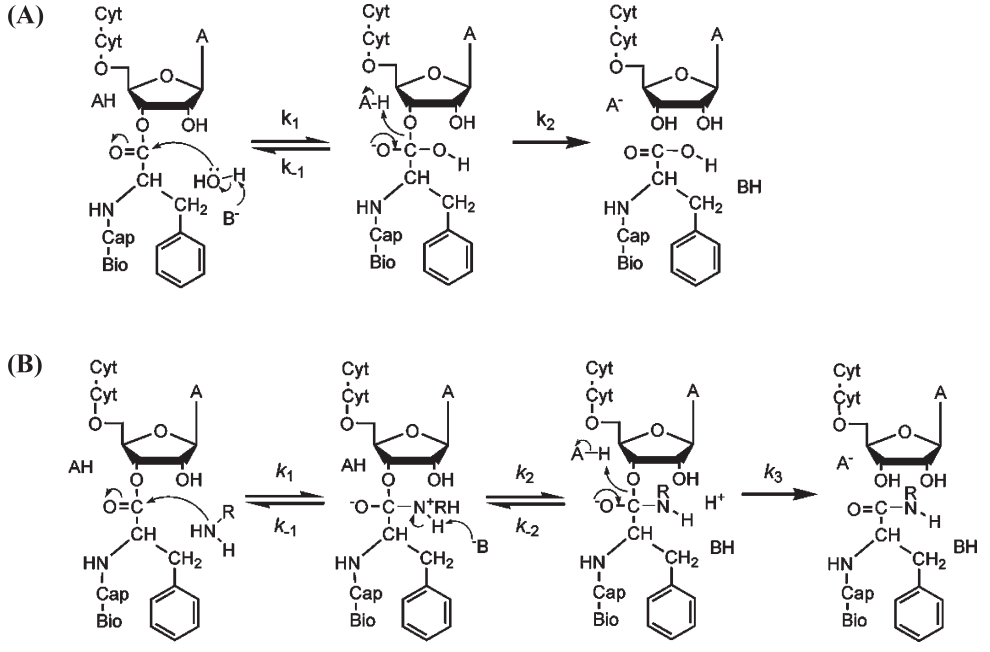

FIGURE 3: Possible reaction mechanisms of CCApcb. (A) Hydrolysis. Attack by hydroxide ion or base-catalyzed attack of water results in the formation of a tetrahedral intermediate. Breaking the ester C−O bond resolves the intermediate into products. In some cases, the intermediate resolves back into reactants. (B) Aminolysis. Amines can attack as neutral species, and the zwitterionic state may be a stable intermediate as shown. Alternatively, one or more steps may be concerted. Because NRH_2 is generally a better leaving group than RO^-, the intermediates will often partition back to substrates.

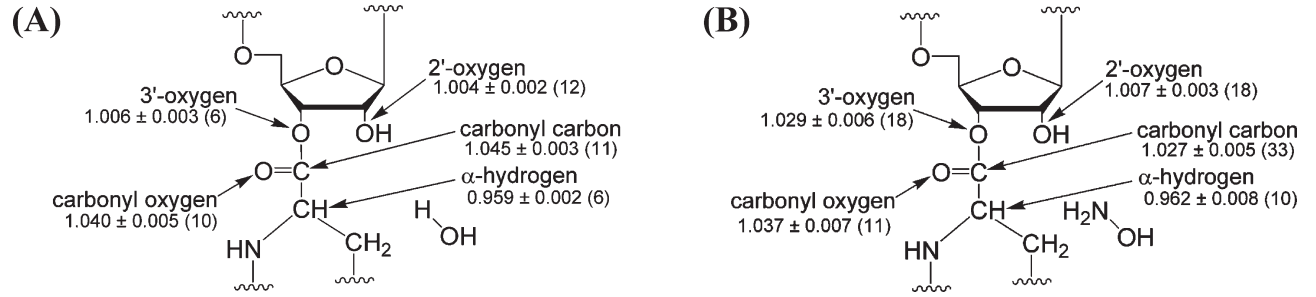

FIGURE 4: Measured isotope effects. Shown are the means and standard deviations, with the number of trials in parentheses, for (A) hydrolysis by water and (B) aminolysis by hydroxylamine.

and k_2, as well as the partitioning of the intermediate (k_2/k_{-1}) (eq 6) (*31*):

$$\mathrm{KIE_{obs}} = \frac{\mathrm{KIE_1}}{\mathrm{KIE_{-1}}} \frac{\mathrm{KIE_2} + (k_2/k_{-1})(\mathrm{KIE_{-1}})}{1 + k_2/k_{-1}} \qquad (6)$$

where KIE_n is the isotope effect on step n. If the intermediate partitions exclusively forward, then the observed isotope effect is equal to the isotope effect on k_1. If the intermediate usually partitions back to reactants, the observed effect is equal to the equilibrium effect ($\mathrm{KIE_1/KIE_{-1}}$) multiplied by the kinetic effect on breakdown ($\mathrm{KIE_2}$). While it is possible that the reaction mechanism is more complicated [especially for aminolysis (see below)], kinetic isotope effects report on only the highest-energy transition states. Therefore, information about multiple steps can be obtained only if they are at least partially rate-limiting (*32*).

Kinetic Isotope Effects on Hydrolysis of CCApcb. Kinetic isotope effects on hydrolysis were determined at pH 8.5 for substitution at the carbonyl carbon and oxygen, the 2′- and 3′-oxygens, and the hydrogen of the amino acid α-carbon (Figure 4A). The measured kinetic isotope effect for the carbonyl ^{18}O substitution is 4.0%. This effect reports on the tetrahedral character of the transition state; the carbonyl bond changes from near double-bond order to near single-bond order in a tetrahedral intermediate. To the best of our knowledge, this is the largest carbonyl ^{18}O effect reported for a reaction of a carboxylic acid ester. For the hydrolysis of methyl formate, methyl benzoate, and *p*-nitrophenyl acetate, carbonyl ^{18}O isotope effects near zero have been observed (*31*−*33*). However, effects of 1.8 and 2.4% have been reported for the hydrazinolysis of methyl benzoate (*31*) and methanolysis of phenyl benzoate (*34*), respectively. Isotope effects at other positions indicated those transition states were relatively late. Therefore, the isotope effects would be expected to be larger for a nearly tetrahedral transition state. Calculations for a model substrate indicate the isotope effect reaches a maximum of approximately 5% for the tetrahedral intermediate. This strongly suggests that the transition state for CCApcb hydrolysis is highly tetrahedral.

The observed effect for deuterium substitution at the amino acid α-carbon is 4.1% inverse (the heavy isotope reacts faster). This effect is also largely dependent on the tetrahedral character of the transition state. The effect is derived from the loss of hyperconjugation between the π electrons of the carbonyl double bond and the σ^* antibonding orbital of the C−H bond. Loss of the π electrons in a tetrahedral-like transition state increases the strength of the C−H bond and leads to an inverse isotope effect. Previous calculations for addition to an aldehyde estimated the most inverse isotope effect is approximately 4% for an extremely tetrahedral transition state (corrected to one deuterium substitution) (*35*). The calculations performed here yield a similar result, with a most inverse value of 4.9%. The comparatively large inverse isotope effect measured here indicates a significant tetrahedral character to the transition state in agreement with the carbonyl ^{18}O effect.

Interpretation of the 2′- and 3′-^{18}O effects is complicated by isomerization of the ester between 2′- and 3′-linkages. By NMR, the ratio of 2′- to 3′-linked ester was determined to be approximately 3:7, in agreement with previous measurements for similar compounds (*26*, *36*). Therefore, the 3′-^{18}O effect is primarily derived from being the leaving group, while the 2′-^{18}O effect is primarily from being vicinal to the leaving group. If the hydrolysis rate of the 2′- and 3′-linked isomers is the same, then the 3′-^{18}O isotope effect is a weighted average of the leaving group and neighboring group effects. The leaving and neighboring group effects can then be deconvoluted from the 2′- and 3′-effects and the equilibrium ratio determined by NMR.

The 3′-^{18}O effect on hydrolysis is 0.6%; this corresponds to a 0.8% leaving group effect. This effect is near the maximum isotope effect expected for the leaving group if formation of the tetrahedral intermediate is rate-limiting (*31*). There is some double-bond character in the ester bond due to resonance with the carbonyl oxygen; the loss of that resonance in a tetrahedral transition state leads to an isotope effect of as much as 1%. Effects ranging from 0.1 to 0.9% have been observed in systems where formation of the tetrahedral intermediate is the dominant rate-limiting step (*31*, *37*). The comparatively large value observed indicates the transition state is largely tetrahedral, in agreement with the other KIEs measured. The maximum isotope effect from breakdown of the tetrahedral intermediate has been estimated to be 6−8% (*31*, *33*). Therefore this step must not contribute substantially to the observed isotope effect, or the transition state for this step is early in breakdown, close to the tetrahedral intermediate.

The 2′-^{18}O effect is primarily derived from its role as the neighboring hydroxyl group. This hydroxyl group increases the rate of hydrolysis of CCApcb by approximately 30-fold (data not shown), similar to the rate enhancement in similar molecules (*15*, *38*). This effect was not observed for lysine-tRNA, possibly because of the different aminoacyl group (*39*). The contribution of the 2′-hydroxyl could be due to orientation effects, proton transfer, or stabilization of the transition state through hydrogen bonds (*38*, *40*). The 2′-^{18}O effect is 0.4%, which corresponds to a 0.3% neighboring group effect.

The primary carbonyl ^{13}C isotope effect is 4.5%. This effect is derived from a number of factors: a decrease in ester C−O bond order, a decrease in carbonyl C=O bond order, and the formation of the C−O bond to water. Even the formation of the C−O bond to water can lead to a normal effect due to reaction coordinate motion. The large normal effect is inconsistent with an early transition state, before there is significant bond order to the nucleophile.

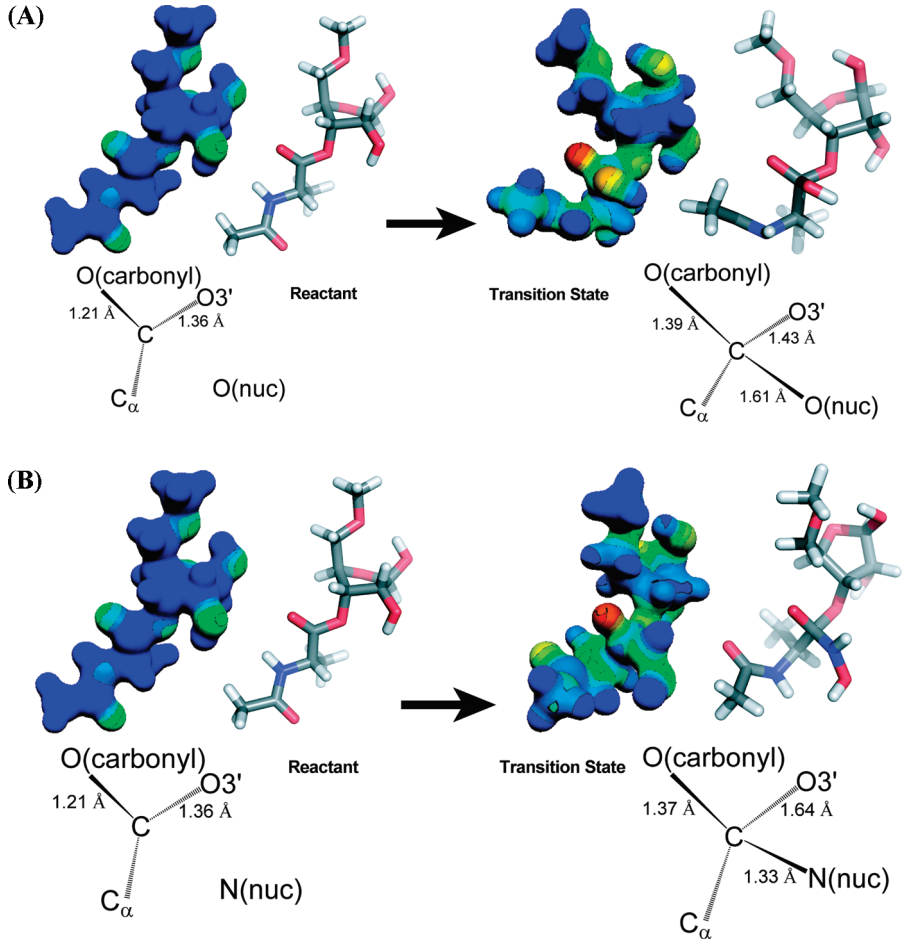

FIGURE 5: Transition state structures. Electrostatic and geometric models of each state are shown side by side in the same orientation. A single transition state is shown for the sake of clarity; the actual reaction pathway is likely to be more complicated. (A) Hydrolysis of CCApcb proceeds through a transition state strongly resembling the tetrahedral intermediate, with an increase in negative charge on the carbonyl oxygen. (B) The aminolysis transition state exists during breakdown of the tetrahedral intermediate, with partial C−O bond breakage and an increase in negative charge at the carbonyl and 3′-oxygens.

To assess the movement of protons at the transition state, the effect of substituting H_2O with a high concentration of D_2O was determined. The measured solvent isotope effect (k_{H_2O}/k_{D_2O}) at 85% D_2O was 1.6 ± 0.5. Transition state hydrogen bonds in the reactions of serine proteases, amidohydrolases, and papain range from approximately 1.7 to 4.0 (*41*). Therefore, the effect observed here, while small, could be derived from a hydrogen bond that is stronger in the transition state than the ground state. The overall effect was too small to determine the solvent isotope effect as a function of D_2O to the accuracy required to determine the number of protons involved.

As a complementary approach, isotope effects were also correlated to the structure of the transition state by starting with a hypothetical structure and predicting isotope effects computationally. The structure was then varied until the calculated isotope effects match the measured ones. The transition state of the hydrolysis reaction was determined using the model shown in Figure 1B. The small 3′-^{18}O experimental KIE of 0.6% for the hydrolysis reaction suggests that the O3′−C bond is fully intact at the transition state, and the near-maximal ^{18}O experimental KIE of 4.0% for the carbonyl oxygen indicates substantial bond order to the nucleophile. This suggests that transition state of the hydrolysis reaction is close to the tetrahedral intermediate. To create a model that matched the measured isotope effects, the transition state was constrained such that there is full bond order between the primary carbon and nucleophile. Therefore, the models of the transition state for the hydrolysis reaction were generated by optimization of structures as intermediates. The transition state models corresponding to tetrahedral or near-tetrahedral transition states gave no imaginary frequencies corresponding to the reaction coordinate. The single imaginary frequency that was observed corresponded to movement of atoms at the 5′-end of ribose, well removed from the reaction center. In subsequent optimizations, the transition state was modeled as an intermediate and EIEs were calculated. The applied constraints were modified further to produce EIEs that closely matched the experimental KIEs. The transition state structure obtained for the hydrolysis reaction by this method closely resembled the tetrahedral intermediate with full bond order to the nucleophile and no cleavage of the 3′-O−C bond (Figure 5A). The transition state structure has a C−OH bond length of 1.61 Å (Table 1). The primary carbon is $sp^{4.81}$ hybridized, and the carbonyl bond mimics a single bond with a length of 1.39 Å. Concomitant delocalization of the carbonyl π electrons results in a significant increase in negative charge at the carbonyl oxygen. The bond between the primary carbon and 3′-O is slightly elongated; the 3′-O−C bond length is 1.43 Å at the TS compared with 1.35 Å in the ground state.

The validity of this computational approach has been quantitatively examined for the epoxidation of alkenes (*42*). While calculations of nonstationary states produce errors in frequency

Table 1: Comparison of Experimental and Theoretical Isotope Effects and Geometric and Electronic Changes in Representative Models of the Reactant and the Transition State for the Hydrolysis Reaction Calculated Using the B3LYP/6-31G** Basis Set

isotope effects			bond properties							
				bond length						
position	experimental	calculated	bond type	RS	TS	bond order change[a] $\Delta(\sigma-\sigma^*)$	RS hybrid[b]	carbon content (%)[c]	TS hybrid[b]	carbon content (%)[c]
carbonyl carbon	1.045 ± 0.003	1.045	C−OH	–	1.61	–	–	–	$sp^{4.81}$	29.5
carbonyl oxygen	1.040 ± 0.005	1.040	C−O	1.21	1.39	−0.896	$sp^{1.99}$	33.9	$sp^{2.49}$	36.8
3′-oxygen	1.006 ± 0.003	1.006	C−O3′	1.35	1.43	−0.036	$sp^{2.56}$	30.5	$sp^{3.45}$	29.0
α-deuterium	0.959 ± 0.002	0.959	C−H	1.10	1.10	0.075	$sp^{3.10}$	64.3	$sp^{3.95}$	60.1

[a]Calculated by subtracting the number of electrons occupying the σ^* orbital from the number occupying the σ orbital and listed as the change between the reactant state (RS) and the transition state (TS). For the carbonyl bond in the RS, electrons in both σ and π bonds were added. [b]Hybridization of the carbon atom. [c]Contribution of the carbon atom to the bond in percent.

determinations, the average deviation between experimental and calculated bond distances was 0.05 Å. It was proposed that the low-frequency modes were most likely to be in error, and these modes do not contribute significantly to the isotope effect. In the case of the hydrolysis reaction here, a single imaginary frequency of 74i cm^{-1} was observed corresponding to the movement of the 5′-methoxy functional group of ribose. This frequency most likely arises from the constraint of this part of the molecule and does not contribute significantly to the calculated isotope effects (Supporting Information). The lack of an imaginary frequency corresponding to the reaction coordinate will introduce some error into primary isotope effects (for instance, the carbonyl carbon effect determined here). However, the structure determined by calculation fits the qualitative aspects identified by comparison with previously studied reactions. Therefore, the true transition state is likely to be similar to the structure calculated here.

Kinetic Isotope Effects on Hydroxylaminolysis of CCApcb. The full set of kinetic isotope effects was also determined for the nucleophilic attack of hydroxylamine on CCApcb at pH 8.5 (Figure 4B). The amino group of hydroxylamine is a much better nucleophile than water, and a significant increase in the rate of CCApcb decomposition is indeed observed. It has been reported that the hydroxyl group of hydroxylamine can also act as a nucleophile (*43*, *44*). To assess this possibility, ^{13}C NMR spectra under several reaction conditions were recorded (Figure 6A). At long time scales, virtually all CCApcb is converted to a product at 170 ppm, with the remainder being hydrolyzed by water. Even if the hydrolysis product were initially formed, we expected that over this time scale it would all convert to the aminolysis product, which is thermodynamically preferred. A ferric chloride test was used to confirm that this is the case (Figure 6B). The aminolysis product is a hydroxamate, which forms a complex with iron upon addition of ferric chloride (*45*, *46*). The characteristic absorbance of this complex in the 450−500 nm range is indeed observed. The same ^{13}C NMR peak is also observed at a short time point, indicating that both the initial (kinetic) product and the final (thermodynamic) products are from aminolysis. A small amount of product resulting from hydrolysis by water is also observed, but there is no evidence of attack by the oxygen of hydroxylamine. This is consistent with a previous report of a single product observed by thin layer electrophoresis whose mobility was consistent with the aminolysis product (*13*). At the concentrations of hydroxylamine used in this study, aminolysis occurs more than 35-fold more rapidly than hydrolysis by water (J. Shaw and R. Green, personal communication). Therefore, the isotope effects were derived overwhelmingly from the aminolysis reaction.

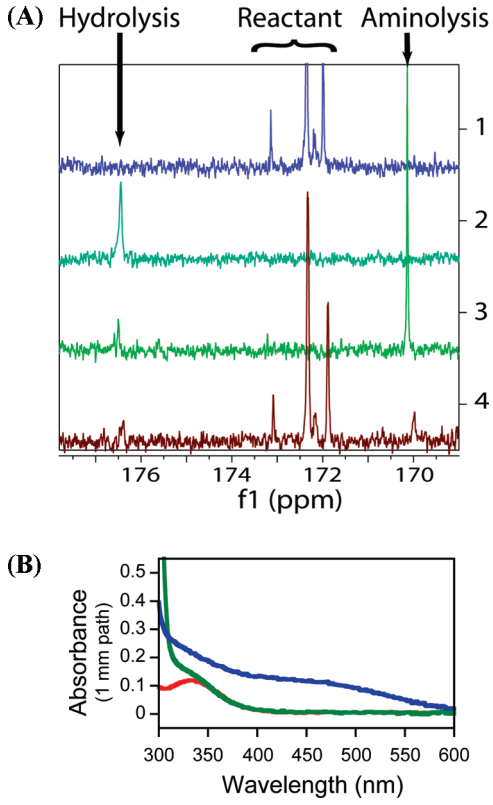

FIGURE 6: (A) ^{13}C NMR of the hydroxylamine reaction. (1) Starting material (CCApcb) in 5% formic acid. A doublet is expected from the 2′- and 3′-isomers. The two smaller peaks appear at low pH. (2) CCApcb allowed to hydrolyze at pH 8.5 for 1 day before the addition of 5% formic acid. (3) CCApcb reacted with 500 mM hydroxylamine for 1 day before the addition of 5% formic acid. (4) CCApcb reacted with 250 mM hydroxylamine for approximately 1 min before the reaction is quenched with 5% formic acid. All peaks in spectrum 4 are identified as the reactant, the water hydrolysis product, or the hydroxylamine aminolysis product. (B) Identification of the 170 ppm peak as the aminolysis product by a ferric chloride test. Spectra of unreacted CCApcb (green) and the product of CCApcb and hydroxylamine (blue) after addition of ferric chloride. The peak for ferric chloride alone (red) is at ~350 nm. The aminolysis product of CCApcb is a hydroxamate, which forms an iron complex with characteristic absorbance around 450 nm.

A plausible mechanism for aminolysis is shown in Figure 3. An extra step is depicted since amines can attack as a neutral species, forming a stable zwitterionic intermediate. Because hydroxylamine is a better leaving group than the 3′-oxygen, the tetrahedral intermediate could resolve back into reactants instead of products (*32*). If the partitioning ratio strongly favors breakdown

Table 2: Comparison of Experimental and Theoretical Isotope Effects and Geometric and Electronic Changes in Representative Models of the Reactant and the Transition State for the Hydroxylaminolysis Reaction Calculated using the B3LYP/6-31G** Basis Set

isotope effects			bond properties							
				bond length						
position	experimental	calculated	bond type	RS	TS	bond order change[a] $\Delta(\sigma-\sigma^*)$	RS hybrid[b]	carbon content (%)[c]	TS hybrid[b]	carbon content (%)[c]
carbonyl carbon	1.027 ± 0.005	1.030	C−N	−	1.330	−	−	−	$sp^{2.47}$	37.3
carbonyl oxygen	1.037 ± 0.007	1.037	C−O	1.21	1.370	−0.898	$sp^{1.95}$	33.8	$sp^{2.70}$	37.5
3′-oxygen	1.029 ± 0.006	1.029	C−O3′	1.36	1.643	−0.217	$sp^{2.59}$	30.3	$sp^{5.67}$	26.5
α-deuterium	0.962 ± 0.008	0.964	C−H	1.10	1.10	0.008	$sp^{3.42}$	63.2	$sp^{3.32}$	62.4

[a]Calculated by subtracting the number of electrons occupying the σ^* orbital from the number occupying the σ orbital and listed as the change between the reactant state (RS) and transition state (TS). For the carbonyl bond in the RS, electrons in both σ and π bonds were added. [b]Hybridization of the carbon atom. [c]Contribution of the carbon atom to the bond in percent.

into reactants, the observed isotope effect is equal to the product of the equilibrium effect on formation of the tetrahedral intermediate and the kinetic isotope effect on its breakdown. This behavior has been observed for other aminolysis reactions with good nucleophiles (*31*, *37*).

The 3′-^{18}O effect was determined to be 2.9% (Figure 4B). Since the 3′-oxygen is the leaving group for only one of the two isomers of CCApcb, this number represents a lower bound for the leaving group ^{18}O effect. Regardless, this effect is significantly larger than that for hydrolysis and is too large to be due to the decrease in bond order in a tetrahedral transition state. Instead, this effect must be derived from the breaking of the ester C−O bond. Leaving group isotope effects of 4.1 and 6.2% have been measured for hydrazinolysis of methyl benzoate and methyl formate, respectively (*31*, *37*). In both cases, breakdown of the intermediate was rate-limiting. The large normal effect indicates that either C−O bond breakage is concerted with C−N bond formation (unlike the mechanism shown in Figure 3) or breakdown of a tetrahedral intermediate is rate-limiting.

A small normal effect of 0.7% was observed for the 2′-^{18}O substitution. Since this includes a large normal factor from the case in which the 2′-oxygen is the leaving group, it is likely that the neighboring group is inverse. The vicinal hydroxyl effect determined from deconvolution is inverse 0.9%. This is a small effect relative to the error in the measurement (0.4%), and the rates of aminolysis of the two isomers may not be equal. However, this result may indicate a prominent role for the 2′-hydroxyl in the aminolysis reaction.

The carbonyl ^{18}O and α-deuterium isotope effects are 3.7% and inverse 3.8%, respectively. While somewhat lower than the maximum expected for a tetrahedral transition state, these effects demonstrate there is substantial sp^3 character to the aminolysis transition state. This is inconsistent with a concerted reaction. The combination of the leaving group ^{18}O, carbonyl ^{18}O, and α-deuterium isotope effects indicates that significant but not complete breakdown of the tetrahedral intermediate has occurred at the transition state for aminolysis.

The carbonyl carbon isotope effect of 2.7% is consistent with the other isotope effects measured. The large normal effect for bond breaking outweighs the small inverse equilibrium effect on the formation of the tetrahedral intermediate.

As with the hydrolysis reaction, a transition state model was varied until the calculated isotope effect matched the experimentally determined ones. In contrast to hydrolysis, the aminolysis reaction has a large 3′-^{18}O KIE of 2.9%, suggesting that there is significant cleavage to the 3′-O−C bond at the transition state. Matching calculated KIEs to the experimental values gave a transition state model for the aminolysis reaction that occurs late along the reaction coordinate (Figure 5B). There is full bond formation between the primary carbon and the attacking nucleophile with a bond length of 1.33 Å (Table 2). The rate-limiting step is cleavage of the 3′-O−C bond, which has a Pauling bond order of 0.73 at the transition state.

Several imaginary frequencies were observed for this model which did not correspond to reaction coordinate motion. As discussed above, these frequencies are likely due to the use of external constraints. Most of these modes do not contribute significantly to the observed isotope effect; however, the largest imaginary frequency has a significant effect on the predicted carbonyl ^{13}C KIE and was included in the KIE calculations (Supporting Information) (*42*).

DISCUSSION

Transition States for Hydrolysis and Aminolysis of CCApcb. To construct a map of the transition state of the uncatalyzed hydrolysis reaction, kinetic isotope effects were determined at several positions at the reaction center. Two different methods were used to correlate observed kinetic isotope effects with transition state structure. First, the observed effects were compared with previously studied reactions. Second, the observed effects were matched to calculated effects for a given transition state structural model. On the basis of these methods, the transition state for hydrolysis of the ribosomal substrate CCApcb very closely resembles the tetrahedral intermediate.

Formation of the tetrahedral intermediate is generally rate-limiting for ester hydrolysis, as observed by isotope exchange, structure−reactivity studies, and kinetic isotope effects (*16*, *47*). If formation of the intermediate is rate-limiting in CCApcb hydrolysis as expected, the transition state determined here is extremely late in that step. This is consistent with the Hammond−Leffler postulate, since the tetrahedral intermediate is higher in energy than the reactants. However, this behavior was not observed for the alkaline hydrolysis of either methyl benzoate or methyl formate. Both transition states were early, based on small deuterium and carbonyl ^{18}O isotope effects (*31*, *48*). This may be due to other structural differences compared with the previously studied esters, for instance, the presence of a 2′-hydroxyl.

In contrast to hydrolysis, the transition state for hydroxylaminolysis of CCApcb occurs during the breakdown of the tetrahedral intermediate. This behavior has often been observed for the reaction of esters with good nucleophiles (*31*, *32*, *37*).

The carbonyl ^{18}O, carbonyl ^{13}C, and α-deuterium effects indicate the reaction is stepwise, with full formation of the bond to the nucleophile preceding scission of the bond to the leaving group. This is likely due to the leaving group; stepwise reactions have also been observed for methyl formate and methyl benzoate, even with hydrazine as a nucleophile (*31*, *37*), while *p*-nitrophenyl acetate reactions are often concerted (*32*). The pK_a of *p*-nitrophenol (approximately 7) is much lower than those of phenol (10), ribose (12), and methanol (15). The improved leaving group character of *p*-nitrophenol destabilizes the tetrahedral structure such that it is no longer a stable intermediate. This is not the case for CCApcb, which conforms to an at least two-step process even with a good nucleophile.

Implications for Release Factor-Catalyzed Hydrolysis. The hydrolysis of CCApcb is chemically identical to peptide release, the final step of protein synthesis catalyzed by the ribosome. This analysis of a model hydrolysis reaction could provide insight into how this reaction is promoted on the ribosome. Recent structures of 70S ribosomes bound to release factors have shown the three-dimensional arrangement of functional groups in the product state (*7*−*9*). However, the mechanism of catalysis is still not clear. The main chain amide of glutamine in the release factor GGQ motif is within hydrogen bonding distance of the 3′-oxygen and therefore has been hypothesized to stabilize the leaving group (*7*). A similar mechanism has been proposed for the Ras protein, which hydrolyzes GTP (*49*). Because uncatalyzed phosphodiester bond cleavage is believed to pass through a dissociative transition state (*50*), stabilizing the leaving group oxygen (which carries a significant negative charge in the transition state) is a potent catalytic strategy. However, the transition state for hydrolysis determined here is associative, with little charge on the leaving group and instead a buildup of negative charge on the carbonyl oxygen (Figure 5). On the basis of models of the 70S ribosome with a transition state inhibitor built into the active site, it was also proposed that the glutamine main chain amide group could stabilize the carbonyl oxygen (*7*). Since this is the location of the buildup of negative charge in the transition state, this mechanism is more likely to be important for catalysis. This is analogous to serine proteases, for which the enzyme stabilizes the transition state carbonyl oxyanion with hydrogen bonds (*51*−*54*).

Implications for Ribosomal Peptide Bond Formation. Peptide bonds are formed by the nucleophilic attack of the α-amino group of aminoacyl-tRNA on the carbonyl carbon of peptidyl-tRNA. The ribosome increases the rate of this reaction by approximately 10^7-fold versus the rates of similar uncatalyzed reactions (*55*). Several mechanisms for this rate enhancement have been suggested, including substrate positioning, electrostatic stabilization, and a role in coordinating proton transfer (*55*−*60*). Measurement of the Brönsted coefficient and kinetic isotope effect of the nucleophile indicated the transition state for ribosomal peptide bond formation differs from that for uncatalyzed aminolysis reactions (*5*, *6*). A comparison of the transition states for ribosomal peptide bond formation and uncatalyzed reactions will be necessary to determine the extent to which chemical catalysis by the ribosome supplements substrate positioning to increase the reaction rate. If the ribosome is responsible for improved proton transfer or for stabilizing particular aspects of the transition state, we expect that the structure of the transition state will be significantly altered.

The transition states for aminolysis of several esters have been determined previously (*31*−*33*, *37*, *48*). However, none of the esters studied contain a vicinal hydroxyl, which is crucial for ribosomal peptide bond formation. Because inclusion of this functional group increases the rate of hydrolysis, it is difficult to measure kinetic isotope effects for aminolysis by a molecule similar to the A-site tRNA. Instead, a better nucleophile, hydroxylamine, was used to ensure the transition state being determined was for aminolysis and not hydrolysis. This results in a later transition state, since nucleophilic attack is not rate-limiting (as it may be for the uncatalyzed attack of A-site tRNA). While this is clearly a weakness of this model system, the measurement of a transition state for aminolysis of a true ribosomal substrate containing a vicinal hydroxyl is an important addition to the previous measurements of similar aminolysis reactions.

For uncatalyzed reactions, it is not believed that the 2′-hydroxyl participates directly in catalysis through donation or abstraction of protons. However, it is possible that in the context of the ribosome, the 2′-hydroxyl plays a more significant role that could be observed through kinetic isotope effects. In fact, the 2′-hydroxyl contributes at least 10^6-fold to peptide bond formation and as much as 1000-fold to peptide release in the context of the ribosome (*4*, *39*), while uncatalyzed reaction rates are generally increased only 30-fold (*15*, *40*).

It has been hypothesized that the ribosome promotes the use of the P-site tRNA 2′-hydroxyl as a proton shuttle (*4*, *56*, *57*). In this mechanism, the 2′-hydroxyl removes a proton from the nucleophilic nitrogen while simultaneously donating its proton to another site. If, as in hydroxylaminolysis, breakdown of the tetrahedral intermediate is rate-limiting, then the proton could be directly transferred to the leaving group. Alternatively, in an earlier transition state such as that observed for hydrolysis, the proton may be transferred to the carbonyl oxygen. In either case, the atom being protonated should have a less normal isotope effect than would otherwise be expected.

In the future, kinetic isotope effects of the ribosome-catalyzed reactions can be compared with those of the previously studied aminolysis reactions lacking the vicinal hydroxyl and with those of the reaction studied here including the vicinal hydroxyl but with a better nucleophile. Differences in the transition states of these reactions will illuminate the role of the ribosome in catalysis.

ACKNOWLEDGMENT

We thank Jared Davis for assistance with NMR, the Keck facility for mass spectrometry, and the reviewers for experimental suggestions.

SUPPORTING INFORMATION AVAILABLE

Information about calculated transition state structures. This material is available free of charge via the Internet at http://pubs.acs.org.

REFERENCES

1. Ban, N., Nissen, P., Hansen, J., Moore, P. B., and Steitz, T. A. (2000) The Complete Atomic Structure of the Large Ribosomal Subunit at 2.4 Å Resolution. *Science 289*, 905–920.
2. Nissen, P., Hansen, J., Ban, N., Moore, P. B., and Steitz, T. A. (2000) The Structural Basis of Ribosome Activity in Peptide Bond Synthesis. *Science 289*, 920–930.
3. Erlacher, M. D., Lang, K., Shankaran, N., Wotzel, B., Huttenhofer, A., Micura, R., Mankin, A. S., and Polacek, N. (2005) Chemical engineering of the peptidyl transferase center reveals an important

role of the 2′-hydroxyl group of A2451. *Nucleic Acids Res. 33*, 1618–1627.
4. Weinger, J. S., Parnell, K. M., Dorner, S., Green, R., and Strobel, S. A. (2004) Substrate-assisted catalysis of peptide bond formation by the ribosome. *Nat. Struct. Mol. Biol. 11*, 1101–1106.
5. Kingery, D. A., Pfund, E., Voorhees, R. M., Okuda, K., Wohlgemuth, I., Kitchen, D. E., Rodnina, M. V., and Strobel, S. A. (2008) An Uncharged Amine in the Transition State of the Ribosomal Peptidyl Transfer Reaction. *Chem. Biol. 15*, 493–500.
6. Seila, A. C., Okuda, K., Nunez, S., Seila, A. F., and Strobel, S. A. (2005) Kinetic Isotope Effect Analysis of the Ribosomal Peptidyl Transferase Reaction. *Biochemistry 44*, 4018–4027.
7. Laurberg, M., Asahara, H., Korostelev, A., Zhu, J., Trakhanov, S., and Noller, H. F. (2008) Structural basis for translation termination on the 70S ribosome. *Nature 454*, 852–857.
8. Weixlbaumer, A., Jin, H., Neubauer, C., Voorhees, R. M., Petry, S., Kelley, A. C., and Ramakrishnan, V. (2008) Insights into Translational Termination from the Structure of RF2 Bound to the Ribosome. *Science 322*, 953–956.
9. Korostelev, A., Asahara, H., Lancaster, L., Laurberg, M., Hirschi, A., Zhu, J., Trakhanov, S., Scott, W. G., and Noller, H. F. (2008) Crystal structure of a translation termination complex formed with release factor RF2. *Proc. Natl. Acad. Sci. U.S.A. 105*, 19684–19689.
10. Frolova, L. Y., Tsivkovskii, R. Y., Sivolobova, G. F., Oparina, N. Y., Serpinsky, O. I., Blinov, V. M., Tatkov, S. I., and Kisselev, L. L. (1999) Mutations in the highly conserved GGQ motif of class 1 polypeptide release factors abolish ability of human eRF1 to trigger peptidyl-tRNA hydrolysis. *RNA 5*, 1014–1020.
11. Seit Nebi, A., Frolova, L., Ivanova, N., Poltaraus, A., and Kisselev, L. (2000) Substitutions of the glutamine residue in the ubiquitous GGQ tripeptide in human eRF1 do not entirely abolish the release factor activity. *Mol. Biol. 34*, 764–765.
12. Zavialov, A. V., Mora, L., Buckingham, R. H., and Ehrenberg, M. (2002) Release of Peptide Promoted by the GGQ Motif of Class 1 Release Factors Regulates the GTPase Activity of RF3. *Mol. Cell 10*, 789–798.
13. Shaw, J. J., and Green, R. (2007) Two Distinct Components of Release Factor Function Uncovered by Nucleophile Partitioning Analysis. *Mol. Cell 28*, 458–467.
14. Kovach, I. M., Belz, M., Larson, M., Rousy, S., and Schowen, R. L. (1985) Transition-state structures for ester aminolysis with and without rate-limiting proton transfer. *J. Am. Chem. Soc. 107*, 7360–7365.
15. Wolfenden, R. (1963) The Mechanism of Hydrolysis of Amino Acyl RNA*. *Biochemistry 2*, 1090–1092.
16. Jencks, W. P., and Gilchrist, M. (1968) Nonlinear structure-reactivity correlations. The reactivity of nucleophilic reagents toward esters. *J. Am. Chem. Soc. 90*, 2622–2637.
17. Blackburn, G. M., and Jencks, W. P. (1968) The mechanism of the aminolysis of methyl formate. *J. Am. Chem. Soc. 90*, 2638–2645.
18. Satterthwait, A. C., and Jencks, W. P. (1974) Mechanism of the aminolysis of acetate esters. *J. Am. Chem. Soc. 96*, 7018–7031.
19. Bender, M. L. (1951) Oxygen Exchange as Evidence for the Existence of an Intermediate in Ester Hydrolysis. *J. Am. Chem. Soc. 73*, 1626–1629.
20. Cleland, W. W. (1995) Isotope effects: Determination of enzyme transition state structure. In Enzyme Kinetics and Mechanism Part D: Developments in Enzyme Dynamics, pp 341−373, Academic Press, New York.
21. Schramm, V. L. (2003) Enzymatic Transition State Poise and Transition State Analogues. *Acc. Chem. Res. 36*, 588–596.
22. Zhong, M., and Strobel, S. A. (2006) Synthesis of the Ribosomal P-Site Substrate CCA-pcb. *Org. Lett. 8*, 55–58.
23. Zhong, M., and Strobel, S. A. (2008) Synthesis of Isotopically Labeled P-Site Substrates for the Ribosomal Peptidyl Transferase Reaction. *J. Org. Chem. 73*, 603–611.
24. Griffin, B. E., Jarman, M., Reese, C. B., Sulston, J. E., and Trentham, D. R. (1966) Some Observations Relating to Acyl Mobility in Aminoacyl Soluble Ribonucleic Acids. *Biochemistry 5*, 3638–3649.
25. Fromageot, H. P. M., Griffin, B. E., Reese, C. B., Sulston, J. E., and Trentham, D. R. (1966) Orientation of ribonucleoside derivatives by proton magentic resonance spectroscopy. *Tetrahedron 22*, 705–710.
26. Wolfenden, R., Rammler, D. H., and Lipmann, F. (1964) On the Site of Esterification of Amino Acids to Soluble RNA. *Biochemistry 3*, 329–338.
27. Caldwell, S. R., Raushel, F. M., Weiss, P. M., and Cleland, W. W. (1991) Transition-state structures for enzymic and alkaline phosphotriester hydrolysis. *Biochemistry 30*, 7444–7450.
28. Frisch, M., Trucks, G., Schlegel, H., Scuseria, G., Robb, M., Cheeseman, J., Montgomery, J., Vreven, T., Kudin, K., Burant, J., Millam, J., Iyengar, S., Tomasi, J., Barone, V., Mennucci, B., Cossi, M., Scalmani, G., Rega, N., Petersson, G., Nakatsuji, H., Hada, M., Ehara, M., Toyota, K., Fukuda, R., Hasegawa, J., Ishida, M., Nakajima, T., Honda, Y., Kitao, O., Nakai, H., Klene, M., Li, X., Knox, J., Hratchian, H., Cross, J., Bakken, V., Adamo, C., Jaramillo, J., Gomperts, R., Stratmann, R., Yazyev, O., Austin, A., Cammi, R., Pomelli, C., Ochterski, J., Ayala, P., Morokuma, K., Voth, G., Salvador, P., Dannenberg, J., Zakrzewski, V., Dapprich, S., Daniels, A., Strain, M., Farkas, O., Malick, D., Rabuck, A., Raghavachari, K., Foresman, J., Ortiz, J., Cui, Q., Baboul, A., Clifford, S., Cioslowski, J., Stefanov, B., Liu, G., Liashenko, A., Piskorz, P., Komaromi, I., Martin, R., Fox, D., Keith, T., Laham, A., Peng, C., Nanayakkara, A., Challacombe, M., Gill, P., Johnson, B., Chen, W., Wong, M., Gonzalez, C., and Pople, J. (2003) Gaussian 03, revision C.02, Gaussian, Inc., Wallingford, CT.
29. Anisimov, V., and Paneth, P. (1999) ISOEFF98. A program for studies of isotope effects using Hessian modifications. *J. Math. Chem. 26*, 75–86.
30. Unrau, P. J., and Bartel, D. P. (2003) An oxocarbenium-ion intermediate of a ribozyme reaction indicated by kinetic isotope effects. *Proc. Natl. Acad. Sci. U.S.A. 100*, 15393–15397.
31. O'Leary, M. H., and Marlier, J. F. (1979) Heavy-atom isotope effects on the alkaline hydrolysis and hydrazinolysis of methyl benzoate. *J. Am. Chem. Soc. 101*, 3300–3306.
32. Hengge, A. C., and Hess, R. A. (1994) Concerted or Stepwise Mechanisms for Acyl Transfer Reactions of p-Nitrophenyl Acetate? Transition State Structures from Isotope Effects. *J. Am. Chem. Soc. 116*, 11256–11263.
33. Marlier, J. F. (1993) Heavy-atom isotope effects on the alkaline hydrolysis of methyl formate: The role of hydroxide ion in ester hydrolysis. *J. Am. Chem. Soc. 115*, 5953–5956.
34. Mitton, C. G., and Schowen, R. L. (1968) Oxygen isotope effects by a noncompetitive technique: The transition-state carbonyl stretching frequency in ester cleavage. *Tetrahedron Lett. 9*, 5803–5806.
35. Hogg, J. L., Rodgers, J., Kovach, I., and Schowen, R. L. (1980) Kinetic isotope-effect probes of transition-state structure. Vibrational analysis of model transition states for carbonyl addition. *J. Am. Chem. Soc. 102*, 79–85.
36. Khym, J. X., and Cohn, W. E. (1954) Identification of the Purine Nucleotides a and b as the 2′- and 3′-Phosphoribosides, Respectively. *J. Am. Chem. Soc. 76*, 1818–1823.
37. Sawyer, C. B., and Kirsch, J. F. (1973) Kinetic isotope effects for reactions of methyl formate-methoxyl-^{18}O. *J. Am. Chem. Soc. 95*, 7375–7381.
38. Bruice, T. C., and Fife, T. H. (1962) Hydroxyl Group Catalysis. III. The Nature of Neighboring Hydroxyl Group Assistance in the Alkaline Hydrolysis of the Ester Bond. *J. Am. Chem. Soc. 84*, 1973–1979.
39. Brunelle, J. L., Shaw, J. J., Youngman, E. M., and Green, R. (2008) Peptide release on the ribosome depends critically on the 2′ OH of the peptidyl−tRNA substrate. *RNA 14*, 1526–1531.
40. Kupchan, S. M., Slade, P., Young, R. J., and Milne, G. W. A. (1962) Intramolecular catalysis. IV: Facilitation of alkaline hydrolysis of alycyclic 1,2-diol monoesters. *Tetrahedron 18*, 499–506.
41. Cook, P. F. (1991) Enzyme mechanism from isotope effects, CRC Press, Boca Raton, FL.
42. Hirschi, J. S., Takeya, T., Hang, C., and Singleton, D. A. (2009) Transition-State Geometry Measurements from ^{13}C Isotope Effects. The Experimental Transition State for the Epoxidation of Alkenes with Oxaziridines. *J. Am. Chem. Soc. 131*, 2397–2403.
43. Jencks, W. P. (1958) The Reaction of Hydroxylamine with Activated Acyl Groups. I. Formation of O-Acylhydroxylamine1. *J. Am. Chem. Soc. 80*, 4581–4584.
44. Mazera, D. J., Gesser, J. C., and Pliego, J. R. (2007) On the mechanism of the reaction between aryl acetates and hydroxylamine. *ARKIVOC* (*Gainesville, FL, U.S.*) *15*, 199–214.
45. Lipmann, F., and Tuttle, L. C. (1945) A specific micromethod for the determination of acyl phosphates. *J. Biol. Chem. 159*, 21.
46. Hulcher, F. H. (1982) Isolation and characterization of a new hydroxamic acid from *Pseudomonas mildenbergii*. *Biochemistry 21*, 4491–4495.
47. Bender, M. L. (1960) Mechanisms of Catalysis of Nucleophilic Reactions of Carboxylic Acid Derivatives. *Chem. Rev. 60*, 53–113.
48. Bilkadi, Z., De Lorimier, R., and Kirsch, J. F. (1975) Secondary α-deuterium kinetic isotope effects and transition-state structures for the hydrolysis and hydrazinolysis reactions of formate esters. *J. Am. Chem. Soc. 97*, 4317–4322.
49. Maegley, K. A., Admiraal, S. J., and Herschlag, D. (1996) Ras-catalyzed hydrolysis of GTP: A new perspective from model studies. *Proc. Natl. Acad. Sci. U.S.A. 93*, 8160–8166.

50. Du, X., Black, G. E., Lecchi, P., Abramson, F. P., and Sprang, S. R. (2004) Kinetic isotope effects in Ras-catalyzed GTP hydrolysis: Evidence for a loose transition state. *Proc. Natl. Acad. Sci. U.S.A. 101*, 8858–8863.
51. Henderson, R. (1970) Structure of crystalline α-chymotrypsin: IV. The structure of indoleacryloyl-α-chymotrypsin and its relevance to the hydrolytic mechanism of the enzyme. *J. Mol. Biol. 54*, 341–354.
52. Robertus, J. D., Kraut, J., Alden, R. A., and Birktoft, J. J. (1972) Subtilisin. Stereochemical mechanism involving transition-state stabilization. *Biochemistry 11*, 4293–4303.
53. Bryan, P., Pantoliano, M. W., Quill, S. G., Hsiao, H. Y., and Poulos, T. (1986) Site-directed mutagenesis and the role of the oxyanion hole in subtilisin. *Proc. Natl. Acad. Sci. U.S.A. 83*, 3743–3745.
54. Joseph, S., Whirl, M. L., Kondo, D., Noller, H. F., and Altman, R. B. (2000) Calculation of the relative geometry of tRNAs in the ribosome from directed hydroxyl-radical probing data. *RNA 6*, 220–232.
55. Sievers, A., Beringer, M., Rodnina, M. V., and Wolfenden, R. (2004) The ribosome as an entropy trap. *Proc. Natl. Acad. Sci. U.S.A. 101*, 7897–7901.
56. Das, G. K., Bhattacharyya, D., and Burma, D. P. (1999) A Possible Mechanism of Peptide Bond Formation on Ribosome without Mediation of Peptidyl Transferase. *J. Theor. Biol. 200*, 193–205.
57. Trobro, S., and Åqvist, J. (2005) Mechanism of peptide bond synthesis on the ribosome. *Proc. Natl. Acad. Sci. U.S.A. 102*, 12395–12400.
58. Trobro, S., and Aqvist, J. (2006) Analysis of Predictions for the Catalytic Mechanism of Ribosomal Peptidyl Transfer. *Biochemistry 45*, 7049–7056.
59. Erlacher, M. D., Lang, K., Wotzel, B., Rieder, R., Micura, R., and Polacek, N. (2006) Efficient Ribosomal Peptidyl Transfer Critically Relies on the Presence of the Ribose 2′-OH at A2451 of 23S rRNA. *J. Am. Chem. Soc. 128*, 4453–4459.
60. Schmeing, T. M., Huang, K. S., Kitchen, D. E., Strobel, S. A., and Steitz, T. A. (2005) Structural Insights into the Roles of Water and the 2′ Hydroxyl of the P Site tRNA in the Peptidyl Transferase Reaction. *Mol. Cell 20*, 437–448.